Dalton Transactions

Accepted Manuscript

This article can be cited before page numbers have been issued, to do this please use: M. C. Gimeno, V. Fernández-Moreira, C. Val-Campillo, I. Ospino, R. P. Herrera, A. Laguna and I. Marzo, *Dalton Trans.*, 2019, DOI: 10.1039/C8DT00298C.

ROYAL SOCIETY OF CHEMISTRY

rsc.li/dalton

ROYAL SOCIETY OF CHEMISTRY View Article Online
DOI: 10.1039/C8DT00298C

Journal Name

ARTICLE

Bioactive and luminescent indole and isatin based gold(I) derivatives

Received 00th January 20xx,
Accepted 00th January 20xx

DOI: 10.1039/x0xx00000x

www.rsc.org/

Vanesa Fernández-Moreira,*[a] Cynthia Val-Campillo,[a] Isaura Ospino, [b] Raquel P. Herrera,[c] Isabel Marzo,[d] Antonio Laguna[a] and M. Concepción Gimeno*[a]

A series of luminescent monometallic [AuL(PPh_3)] (**1**-**3**) and bimetallic [Au_2(μ-dppe)L_2] (**4**, **6**, **8**) and [Au_2(μ-dppp)L_2] (**5**, **7**, **9**) complexes, where L is either 4-cyano-indole, isatin, or 5,7-dimethyl-isatin, and dppe and dppp are 1,2-bis(diphenylphosphino)ethane and 1,3-bis(diphenylphosphino)propane, respectively, have been synthesised. X-ray diffraction confirmed the tendency to establish aurophillic interations for those complexes containing dppe. Luminescent studies and theoretical calculations revealed a different origin for both families, i.e. indole and isatin species. Thus, indole derivatives presented a ligand-to-ligand-charge-transfer transition (LLCT) from the indole to the PPh_3 fragment, whereas for the isatin derivatives an intraligand–charge-transfer transition (ILCT) within the isatin fragment is proposed. In both cases the gold centre slightly implicated as a ligand-to-metal-charge transfer transition (LMCT) (from the indole/isatin to Au(I)). Cell antiproliferative assays in lung cancer cells (A549), leukemia Jurkat-pLVTHM and Jurkat-shBak cells (cisplatin sensitive and resistant respectively) showed excellent cytotoxic values (10.11 - 0.28 μM), resulting the leukemia cells the most sensitive and the bimetallic species the most active agents. Preliminary studies associated the cytotoxicity to a combination of diferent factors, being the metallic fragment the main responsible. Remarkably, these complexes are able to inhibit the cellular growth of cisplatin resistant Jurkat-shBak cells highlighting their promising future as an alternative anticancer agent.

Introduction

Indole has become one of the most privileged structural motif in drug discovery and it exists in a great number of active natural and non-natural products.[1] Its interesting properties cover diverse research areas such as pharmaceuticals, fragrances, agrochemicals, pigments, and material science being many of these compounds already drugs on market or compounds in clinical trials (Figure 1).[2] The importance attained by the indole derivatives and their broad scope of applications justifies its appellation as the *"The Lord of the Rings"* of the aromatic compounds.[3] Therefore, the design of new indole structures with appealing properties is still an active challenge and the goal of considerable efforts by many research groups.[4]

Other related structure is the isatin skeleton which has gained much attention from organic and medicinal chemists, since this motif also constitutes the structural core of a great number of natural products as well as several other drug candidates (Figure 1).[5] Together with all this broad spectrum of biological properties,[6] indole and isatin derivatives also play an important role in bioluminescence. Therefore, their light emission properties have become subject of research, although less explored than their bioactivity but sometimes associated to this.[7] On the bases of our continuous search on the development of new biologically active gold complexes[8] and their combination with luminescent fragments[9] in order to to be used as emissive tags, the exploration of new indole and isatin gold based derivatives could be an excellent approach for delivering novel bioactive metallodrugs.

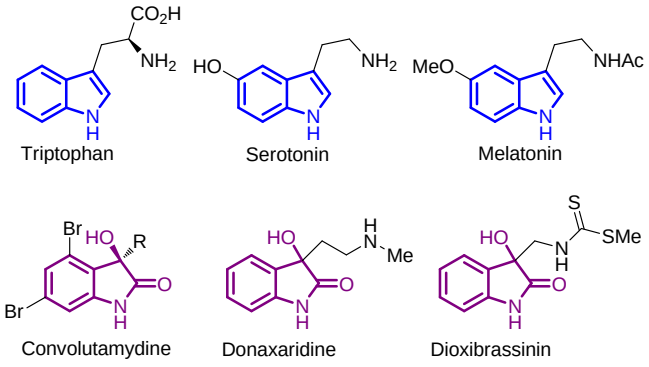

[a] Departamento de Química Inorgánica, Instituto de Síntesis Química y Catálisis Homogénea (ISQCH), CSIC-Universidad de Zaragoza, 50009 Zaragoza, Spain
E-mail: vanesa@unizar.es, gimeno@unizar.es
[b] Departamento de Química Aplicada, Universidad Pública de Navarra - Edificio Los Acebos, 31006 Pamplona, Spain.
[c] Departamento de Química Orgánica, Instituto de Síntesis Química y Catálisis Homogénea (ISQCH), CSIC-Universidad de Zaragoza, 50009 Zaragoza, Spain
[d] Departamento de Bioquímica y Biología Celular, Universidad de Zaragoza-CSIC, 50009 Zaragoza, Spain

† Footnotes relating to the title and/or authors should appear here.
Electronic Supplementary Information (ESI) available: [details of any supplementary information available should be included here]. See DOI: 10.1039/x0xx00000x

Fig 1. Selection of indole and isatin derivatives biologically active.

View Article Online
DOI: 10.1039/C8DT00298C

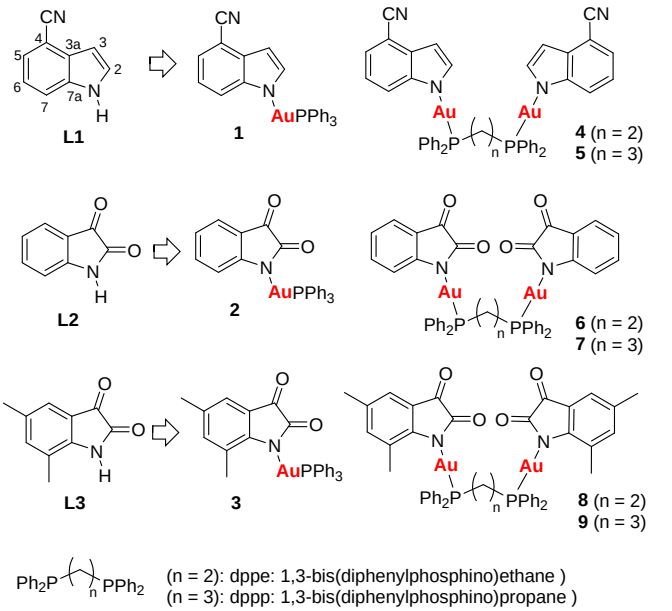

Fig 2. Representation of **L1**-**L3** and their corresponding monometallic **1-3** and bimetallic **4-9** gold(I) complexes. Numbering for the NMR assignments is depicted for **L1**.

In spite of the increasing number of bioactive indole compounds found in the literature, it is noticeable that there are scarce examples of indole or isatin derivatives bonded to gold[10] and only a couple of them dealing with the cytotoxic activity.[10c,10d] Recent investigations dealing with gold complexes containing azaindoles reveal their great potential as an alternative to cisplatin for the treatment of ovarian carcinoma, in particular in A24780 carcinoma cell.[11] Similarly, other gold complexes containing in their structure fussed heterocyclic N-donor ligands, such as purine,[12] adenine[13] or xanthine,[14] i.e. similar structures to those of indole or isatin, expose their incredible prospective as partners of bioactive gold(I) species. For that reason, we intend to evaluate the antitumor activity of a variety of indole and isatin based gold complexes, as well as their luminescence for their plausible use in cell imaging. The antitumor properties of gold derivatives with nitrogen-based ligands have been more extensively studied for gold(III).[15] However, not many examples have been described for gold(I), which is mainly dominated by sulfur, carbon or phosphine type ligands.[16] This is the first study of the antitumour properties of indole and isatin based gold derivatives. Therefore, this study would contribute to widen the knowledge regarding the bioactivity of gold(I) complexes containing N-donor ligands.

Results and Discussion

Three representative structures were selected for this investigation; 4-cyanoindole **L1**, isatin **L2** and 5,7-dimethylindoline-2,3-dione **L3**. Thus, **L1** bearing a nitrile group provides an easily transformable site to different functionalities, among others, to acid or aldehyde groups which could be useful intermediates for different structures.[17] The isatin **L2** is the structural core of the many bioactive compounds,[5] and the **L3** derivative is also present in diverse important biological structures.[18]

Synthetic procedure and characterization

Monometallic gold(I) complexes (**1**-**3**) were synthesised by reaction of the corresponding indole or isatin derivative **L1**-**L3**, Figure 2, with [AuCl(PPh$_3$)] in presence of Cs_2CO_3 to assist the amine deprotonation. The same synthetic procedure was followed for the synthesis of bimetallic complexes (**4**-**9**), using either [Au_2Cl_2(μ-dppe)] or [Au_2Cl_2(μ-dppp)] instead of [AuCl(PPh$_3$)], being dppe: 1,2-bis(diphenylphosphino)ethane and dppp: 1,3-bis(diphenylphosphino)propane. Spectroscopic characterisation of each complex was performed by IR, ^{1}H, ^{31}P{^{1}H} and ^{13}C{^{1}H} NMR spectroscopy and the most relevant data are collected in Table 1. Infrared spectroscopy showed in all cases the disappearance of the υ(N–H) stretching bands at ca. 3320 cm^{-1} for the 4-cyanoindole derivatives and 3188 cm^{-1} in the case of isatin derivatives, indicating the deprotonation of the amine groups and further coordination to the gold fragment.

Table 1. Selected IR frequencies and ^{31}P, ^{1}H and ^{13}C NMR chemical shifts for **L1**-**L3** and complexes **1**-**9**. IR spectra were measured in solid state and NMR spectra recorded in $CDCl_3$. Experimental data for complex **2** reported somewhere else.[19]

	IR / (cm^{-1})	^{31}P{^{1}H} NMR / (ppm)	^{1}H NMR / (ppm)	^{13}C NMR / (ppm)
L1	2230, 2014[a]	-	6.78[c]	138.6[h]
L2	1745, 1724, 1613[b]	-	6.92[d]	150.7[g]
L3	1729, 1613[b]	-	7.20[e]	147.1
1	2213[a]	31.3	6.76-6.74[c]	144.6[f]
3	1719, 1679, 1615[b]	32.1	7.13[e]	157.6[f]
4	2208[a]	30.4	6.75[c]	-
5	2208[a]	23.4	6.68[c]	144.5[f]
6	1726, 1682, 1601[b]	26.6	6.76[d]	160.7[f]
7	1726, 1682, 1602[b]	25.4	6.80-6.70[d]	161.7[f]
8	1730, 1669, 1616[b]	27.4	6.76[e]	156.9[f]
9	1722, 1678, 1615[b]	25.0	6.81[e]	157.2[f]

[a] ν(CN), [b] ν(CO), [c] δ(*CH*(3)), [d] δ(*CH*(7)), [e] δ(*CH*(4)), [f] δ(*C*(7a)), [g] δ(*C*(7a)) in DMSO-d$_6$, [h] δ(*C*(7a)) in $CDCl_3$.

In addition, the characteristic strong υ(C≡N) stretching band of 4-cyanoindole that appears at 2230$_{(sh)}$ and 2214 cm^{-1} is shifted to 2213 cm^{-1} (compound **1**) and 2208 cm^{-1} (complexes **4** and **5**) upon complexation, presenting also a considerably intensity decrease. Moreover, the IR spectrum of **L2** and **L3** presented strong absorptions in the carbonyl region at c.a. 1745, 1724 and 1613 cm^{-1} that are shifted to lower frequencies when the coordination reaction takes place, i.e. around 1726, 1682 and 1601 cm^{-1}.[10b] Further spectroscopic data provided by ^{31}P NMR spectra measured at room temperature exhibited only one resonance. The typical chemical shift for a PPh$_3$P-Au-N environment was observed in the range 30-32 ppm and at highfield those corresponding to the bimetallic species.[20] In

addition, dppp derivatives, i.e. species **5**, **7** and **9**, displayed the lowest phosphorous chemical shift which can be attributed to small variations in the dihedral or bond angles promoted by the different number of methylene spacers among the two phosphorous atoms.[21] Moreover, chemical shifts observed in $^{13}C\{^{1}H\}$ NMR and ^{1}H NMR spectroscopy also corroborated the success of the complexation reaction. Thus, complexes **1–8** showed a deshielding effect of the *C*(7a) as a result of the coordination of **L1**, **L2** and **L3** to the gold fragments. Specifically, the *C*(7a) chemical shift is observed at ca. 144, 157 and 161 ppm for the different gold families respectively. Moreover, phenyl carbon atoms are well defined in the ^{13}C NMR, exhibiting magnetically inequivalent atoms for the dppe derivatives. As a result, complexes **4**, **6** and **8** presented pseudo-triplets ("t") for *meta* and *ortho* carbons, i.e. doublets of doublets with $J_{pc} = J_{pc'}$ = 6-7 Hz, similar to those seen in analogous complexes.[20] This magnetic inequivalence is not unexpected due to the symmetry of the molecule.[22] In addition, the disappearance of the signal belonging to N–H protons together with the chemical shifts presented by the most characteristic protons of **L1** (C*H*(3)), **L2** ((C*H*(7)), and **L3** (C*H*(4)) evidences the successful formation of the desired gold complexes **1**-**9**. In addition, stability of the complexes was tested for selected species (compound **6**) in a highly coordinative solvent, DMSO-d_6, by ^{1}H and ^{31}P-NMR spectroscopy, see Figure S1. The experiment showed that complex **6** was able to remain unaltered for at least 24h under those conditions. Electrospray ionisation mass spectroscopy (ESI-MS) was used to analyse the fragmentation of the molecules. Unfortunately, molecular ions were only observed for complexes **1**, **3** and **4**. Instead, all other compounds displayed the typical fragmentation pattern where one of the ligands (**L1**, **L2** or **L3**) is lost. The stability of the complexes in DMSO solution is comprised by the presence of PBS buffer after 6 hours, but it is not up to 24h when a clear The stability of complexes Interestingly, crystals of **6**, **7** and **8** suitable for X-ray analysis were obtained by slow diffusion of either ether or hexane into a solution of acetone or dichloromethane.

X-ray Crystallography

Single crystals suitable for X-ray diffraction analysis of complexes **6**, **7**, **8** were obtained by slow diffusion of either ether or hexane into a solution of the complex in dichloromethane (DCM) or acetone, (see Figures 3 and 4). They presented a tetragonal, triclinic and monoclinic crystal system, respectively, and the asymmetric unit is formed by half molecule of **6**, one of **7** and two independent molecules of **8**, Table S1. Only compound **6** bears crystallisation solvent molecules trapped in their crystalline structure (DCM and H_2O). All of them presented the typical bond lengths and distorted linear disposition around the metal centre. Thus, Au-P distances range from 2.229(3) to 2.241(3) Å, Au-N distances are between 2.047(8) and 2.057(4) Å and N-Au-P angles lie among 170.5(2) and 179.25(13)°.[10a,19,23] A summary of most significant bond distances and angles is collected in Figure 3 and 4. Aurophilic interactions were observed in the case of the bimetallic complexes **6** and **8**.[24] Possibly, the presence of the dppe as the bridging ligand instead of dppp is allowing these interactions take place. Therefore, folding of dppe renders a c-shape disposition where coordinated gold atoms are within the range of stablishing intramolecular gold interactions and the subsequent structure stabilization. Torsion angles of the system P-C-C-P are 33.5(3)° (**6**), 75.1(9)° (**8A**) and 104.6(7)° (**8B**). Instead, dppp does not offer such possibility and its methylene chain prefers to adopt an extended disposition, (see Figure 3). Specifically, the Au-Au distance observed for molecules **6** and **8A** and **8B** are 3.0141(6) and 3.0058(5) and 3.1136(6) Å respectively values in the range of aurophilic interactions.[24] Moreover, offset- π-π interactions between the parallel fused phenyl rings of the isatin units are also seen for complexes **6** and **8A** and **8B.** Centroid-centroid distances are 3.660, 3.689, 3.600 Å, respectively, and the angle between the perpendicular line to the phenyl and the centroid-centroid vector ranges from 19.01 to 22.30°, see Figure S2-S4.[25]

In the particular case of compound **8**, short contact interactions among the two independent molecules of the asymmetric unit are also revealed. Hence, the specific intermolecular interactions are those stablished between H95···C6 (2.285 Å), H95···H18B (2.373 Å), O5···H17A (2.506 Å) and H112···C25 (2.796 Å), Figure S5. None hydrogen bond interaction is observed. Alternatively, the linearity of compound **7**, due to the bridging dppp ligand, causes that the gold atoms are located in the furthermost position and no additional intramolecular interactions between the isatin unit and/or the phenyl rings are found.

View Article Online
DOI: 10.1039/C8DT00298C

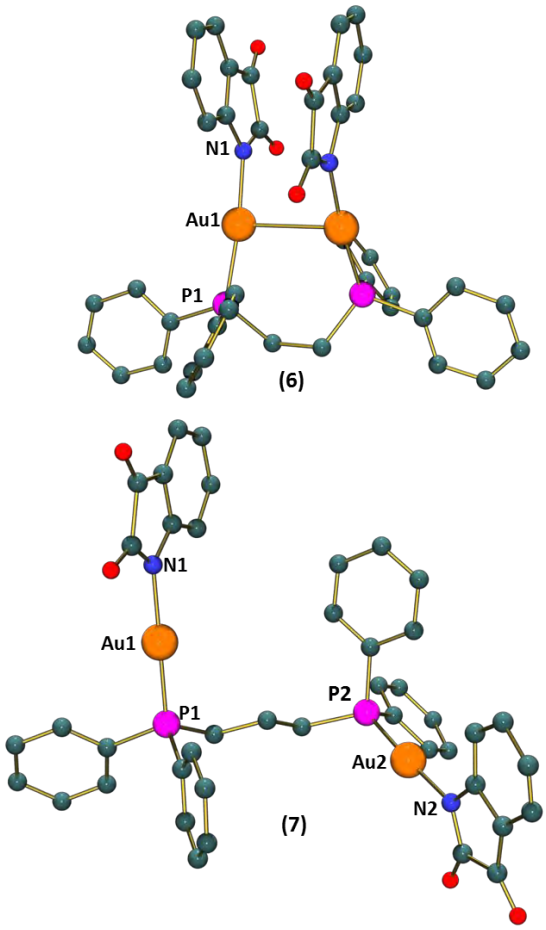

Fig 3. Depiction of the molecular structure of complexes **6** and **7** and a summary of their most relevant bond length (Å) and angles (°). Complex **6**: Au1-P1 2.2401(16), Au1-N1 2.050(7), Au1-Au1 3.0141(6); N1-Au1-P1 174.19(15). Complex **7**: Au1-P1 2.2362(13), Au1-N1 2.057(4); N1-Au1-P1 179.25(13), Au2-P2 2.2403(12), Au2-N2 2.086(7); N2-Au2-P2 172.3(3).

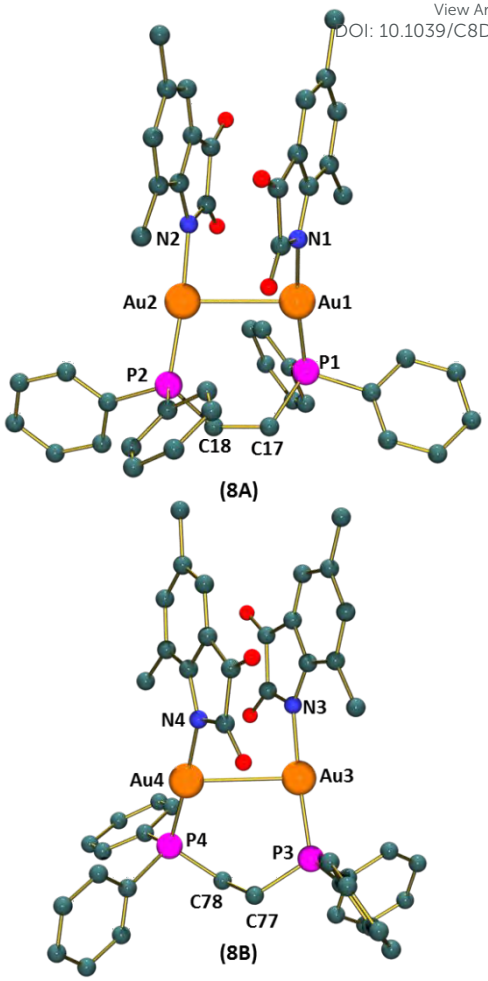

Fig 4. X-ray representation of the molecular structure of complex **8** and summary of their most relevant bond lengths (Å) and angles (°). Molecule **8A**: Au1-P1 2.239(2), Au1-N1 2.065(7), Au1-Au2 3.0058(5), Au2-P2 2.241(3), Au2-N2 2.047(8), N1-Au1-P1 170.5(2), N2-Au2-P2 175.1(2). Molecule **8B**: Au3-P3 2.237(2), Au3-N3 2.048(8), Au3-Au4 3.1136(6), Au4-P4 2.229(3), Au4-N4 2.056(8); N3-Au3-P3 173.0(3), N4-Au4-P4: 176.2(2).

Photophysical properties

UV-visible absorption spectra of complexes **1**-**9** were recorded in a DCM solution at 298 K and the most relevant data are summarised in Table 2. The absorption spectra of complexes **1**-**9** showed an intense absorption band at *ca.* 235 nm that can be attributed to ligand centred transitions, π→π* among **L1**, **L2**, **L3** and also among the phenyl units. Moreover, the less intense bands at lower energies are thought to be n→π* transitions within the cyano or carbonyl group and the N-C of the heterocycle, see Figure S6.[26] Emission and excitation spectra were also recorded for **1**-**9** in DCM solution as well as for **L1**, **L2** and **L3** for comparison purposes. The emission maxima of the ligands differ completely upon their chemical nature (Figure 5). Thus, **L1** presented an emission maximum at 365 nm and **L2** and **L3** at 524 and 554 nm, respectively. For both families, these emissions can be assigned to IL transitions, where their different electron density plays an important role on the HOMO and LUMO energy levels.[27] In contrast, complexes **1**-**9** presented a similar behaviour, featureless

View Article Online
DOI: 10.1039/C8DT00298C

emission bands with an emission maximum between 371 and 429 nm. Specifically, complexes **1**, **4** and **5** displayed an emission band centred at c.a. 407 nm implying a shift to lower energy compared to their precursor **L1**. In contrast, complexes **2**, **3** presented an emission at 383 and 371 nm and their analogous bimetallic species at 398 nm and at c.a. 424 nm exhibiting a considerable shift to higher energies from their correspondent uncoordinated ligands **L2** and **L3**. The fact that the emission maxima of **1**-**9** are similar, with variation of only 58 nm, contrasting with that observed for **L1**, **L2** and **L3** of 189 nm, suggests that the gold-phosphine fragment must have some sort of implication in the electronic transition. Taking into account the emission values seen for **1**-**9**, all of them close to 400 nm, an emission derived from a mixture of LLCT and LMCT transition could be proposed, where possibly the LLCT transition has a higher contribution because of such high energy emission value. Moreover, the low lifetime displayed by all the complexes (0.156-0.721 μs) suggest that the participation of the metal centre in the transition, if there is one, it would be small. These lifetime values are typical from a fluorescent transition which is in concordance with the small Stokes shift seen, from 35 to 70 nm, see Figure S7.[28] Moreover, it is also worth noticing that the aurophilic interactions seen in solid state for complexes **6** and **8** are not maintained in solution, as none emission, *ie.* MMCT transition, at lower energy (c.a. 600 nm) is seen that might suggest otherwise. As a result, the photophysical properties of the mono- and bimetallic species are alike.

Table 2. Absorption, emission, excitation and lifetimes of complexes **1**-**9** measured in DCM at 298K. (λ_{em}/nm (λ_{exc} / nm): **L1**, 365 (337); **L2**, 524 (337); **L3**, 554 (353).

	UV-vis (×10⁴ ε/dm³ mol⁻¹ cm⁻¹)	λ_{em}/nm (λ_{exc} / nm)	ζ / μs
1	231(67000), 276(19800), 305(16200), 341(10800)	407 (337)	0.174
2	245(38400), 260(26200)	383 (337)	0.178
3	245(30400), 270(14600), 300(3000)	371 (331)	-
4	230(132400), 275(37000), 303(25000), 350(5000)	407 (373)	0.156
5	232(94200), 273(29800), 304(23400), 341(1000)	407 (376)	0.197
6	230(106000), 249(58200), 259(42400), 276(30000), 305(11800)	398 (338)	0.721
7	242(66600), 276(15400)	398 (342)	0.638
8	241(69200), 255(58400), 268(33000), 305(13200), 442(2400)	429 (359)	0.211
9	237(127600), 255(110600), 311(21000), 451(4000)	424(355)	0.198

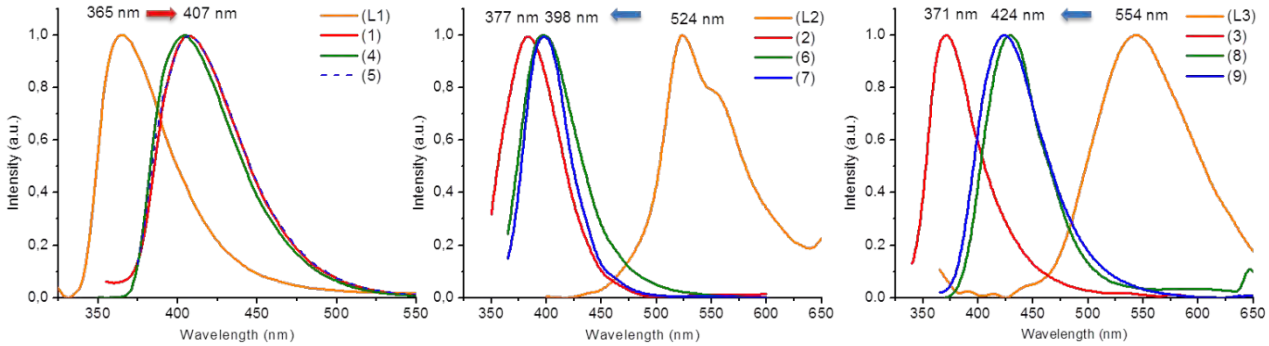

Fig 5. Emission spectra of **L1**-**L3** and complexes **1**-**9** measured in DCM solution.

Theoretical calculations

In order to gain insight into the different photophysical behaviour observed for **L1**-**L3** and **1**-**9**, we carried out DFT and TD-DFT calculations on representative systems, specifically **L1**, **L2**, **1 (L1Au)** and **2 (L2Au)**. We analised their electronic structure and electronic transitions. Each structure were fully optimised in the ground state at the DFT level using the PBE1PBE functional. The solvent effects were performed using the IEFPCM approach considering the noncoordinant solvent, dichloromethane. Frequency calculations were also performed and their positive value confirms the stability of the optimised geometry. Moreover, the optimised parameters of the selected species are in agreement with the experimental data of analogous systems (See Figure S8 and Table S2 of Supporting Information).[29]

The energy gap (ΔE_{H-L}) is the energy difference between the highest occupied molecular orbital (HOMO) and lowest unoccupied molecular orbital (LUMO) and it is largely responsible for the chemical and spectroscopic properties of the molecules.[30] Theoretically calculated frontier molecular orbitals in the ground state including HOMO–LUMO energy levels and energy gap are illustrated in Figure 6. **L2** has a smaller energy gap than **L1**. Hence the eventual charge transfer occurs easier for isatin species, **L2**, which correlates with the emission maxima seen experimentally (524 nm for **L2** and 365 nm for **L1**). This band has been reported as an intra-

ligand charge transfer transition (ILCT). The distributions of electron density of HOMO and LUMO orbitals of **L1** and **L2** predominantly moves in the fragment -NHCRCR- (R= H or O), indicating an increase in the charge transfer character of the transition on going from **L1** to **L2**.

The Au(I) complexes reported in this study are luminescent, they emit in the blue region of the spectrum. The presence of low-energy emission and absorption bands in the electronic spectra, support the assignment of the luminescence to a LMCT but it is not clear the role of the metal. To gain insight into the nature of the orbitals of the complexes and the relative trends in orbital energies according to their respective ligands, molecular orbital calculations were carried out for complexes **1** (**L1Au**) and **2** (**L2Au**). When the metal fragment is coordinated to **L1** and **L2**, a decrease in the HOMO-LUMO gap energy was observed. This could be due to a strong energy destabilisation of the HOMO and LUMO orbitals in all cases (**L1Au** and **L2Au**). For complex **1** the emission band is shifted to lower energy compared to their precursor **L1**. In contrast, complex **2** presented a considerable shift to higher energies from their correspondent ligand **L2**. These shifts in energy of the different complexes indicate the participation of orbitals of the different ligands. The calculated HOMO and LUMO of **1** and **2** are shown in Figure 6. In the case of **1**, the HOMO consists mainly of indole ligand orbitals (97%) whereas the LUMO is formed by a contribution from the PPh_3 ligand (97%). Both HOMO and LUMO have a slightly participation of the gold metal (3%). Therefore, in the eventual transition an alternative assignment must be considered, an indole-ligand to PPh_3-ligand charge transfer (LLCT) with a small contribution of the gold metal.

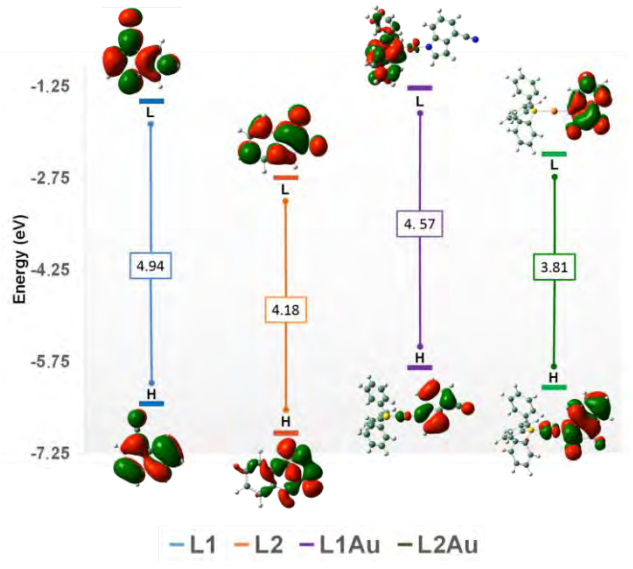

Fig 6. Frontier molecular orbitals and ΔE_{H-L} for **L1**, **L2**, **L1Au** and **L2Au**. H and L denote the highest occupied and lowest unoccupied molecular orbitals, respectively.

In the case of complex **2**, its HOMO is mainly located in the orbitals of the isatin ligand (93%) and gold metal (7%), whereas the LUMO has high participation of isatin ligand orbitals (98%). In contrast with complex **1**, there is no contribution from the PPh_3 ligand. Consequently, the emissive behaviour of complex **2** could be assigned to ligand to metal charge transfer (LMCT) mixed with intraligand charge transfer (IL-CT) (isatin centred) with some contribution from the metal.

Biological activity.

The antiproliferative properties of complexes **1**-**9** were assessed in several cancer cell lines, i.e. lung A549 cells and leukemia Jurkat-pLVTHM and Jurkat-shBak cells, by monitoring their ability to inhibit cell growth using the MTT assay. Jurkat-pLVTHM and Jurkat-shBak cells are known to be cisplatin sensitive and resistant cells, respectively.[31] Therefore, the results here presented will provide additional information regarding the cytotoxicity of the complexes **1**-**9** in cancer cells where the cisplatin has no use, with the expectation of presenting them as an alternative treatment. The results of these tests are summarised in Table 3. There is a clear trend in the cytotoxic activity of the different complexes in the three cell lines. Bimetallic species **4**-**9** are able to inhibit much more the proliferative activity than the monometallic species **1-3**, reaching IC_{50} values up to 19 times smaller, as for instance in the case of IC_{50}(**3**) = 9.09 ± 1.19 *vs* IC_{50}(**8**) = 0.48 ± 0.05 µM in Jurkat-shBak cells. The same trend have been observed for the indole family in HeLa cells, see caption of table 3. It is important to point out the role of gold coordination for achieving certain antiproliferative effect as none of the ligands, **L1**-**L3**, presented any cytotoxicity in A549 cells at the measured concentrations by themselves (IC_{50} > 100 µM). In addition to them, [Au(indole)PPh_3] was also tested to elucidate any possible influence of indole or isatin substituents within the cytotoxic activity. However, the similar IC_{50} values found for **1**-**3** and [Au(indole)PPh_3] in the three cell lines revealed a low influence of the substituents on the antiproliferitive activity. It is crucial to notice that diphosphine derivatives such as dppe have been already proved to bear cytotoxic by itself.[32] Therefore, the higher antiproliferative effect exhibited by the bimetallic species in comparison with that of the monometallic could be assigned to a cooperative effect between the presence of two gold centres and the diphosphine fragment. To support this idea, the antiproliferative activity of dppe and dppp was measured in Jurkat-pLTVHM cells giving IC_{50} values close to 50 µM. Such high IC_{50} values point towards the metal centre as the main responsible for cytotoxicity, possibly targeting the thioredoxin reductase (TrxR) by comparison with multiple examples on gold complexes reported in the literature.[33] Additionally, both leukemia cell lines were sensitive to the action of **1–9**, contrasting with the non-antiproliferative character of cisplatin in Jurkat-shBak cells,[34] and proposing these gold species as a new source of an alternative treatment to cisplatin. Alternatively, cytotoxicity of selected complexes (**1**, **2**, **4** – **6**) was examined in a non-cancerous cell line, MEF cells (mouse embryo fibroblast), see table 3. Despite that this preliminary analysis revealed also a high antiproliferative character, their selectivity towards cancer cells cannot be ruled out as mouse embryo fibroblast

View Article Online
DOI: 10.1039/C8DT00298C

are not comparable to human healthy cells. Additionally, inhibition of the thioredoxin assay was performed for complex **6**. Specifically, A549 cells were treated with **6** (DMSO) for 4 h. Then, total protein extracts were prepared and used for the determination of thioredoxin activity. Subsequently, the artificial substrate 5,5'-dithiobis-(2-nitrobenzoic acid) (DTNB) was added. DTNB would rapidly evolve to two molecules of 2-nitro-5-thiobenzoaye anion (TNB) if thioredoxin redutase is in the presence of NADPH. Thus, the reduction of DTNB to TNB affords a yellow colour that can be detected at 412 nm by UV-absorption.[35] The evolution of the TNB formation was recorded for 5 min and compared with that of a control assay. As a result of the comparison, no inhibition of the thioredoxin was observed, see Figure 7. This result was further corroborated by a preliminary analysis on the production of reactive oxygen species (ROS) in colorectal adenocarcinoma cells (CACO cells). Once again, incubation of complex **6** with CACO cells did not promote the production of ROS postulating the existence of a different biological target than that of thioredoxin.

Finally, stability of the complexes was analysed for selected species, complexes **2** and **6** in mixtures of PBS:DMSO and DEMEM:DMSO (0.05%) by UV-absorption spectroscopy, see figure S9. In both cases the complexes remained intact up to 6 h, after that a new absorption band was observed over 350 nm as a result of the formation of new species.

Table 3. IC_{50} values of complexes **1-9** measured by an MTT assay after 24h incubation in A549, Jurkat-pLTVHM, Jurkat-shBak and MEF cells.

	A549	Jurkat-pLTVHM	Jurkat-shBak	MEF
1	6.50 ± 2.30	7.61 ± 1.57	4.41 ± 0.93	0.22 ± 0.01
2	10.11 ± 7.61	2.89 ± 1.07	4.45 ± 1.80	1.80±0.28
3	6.89 ± 1.25	6.34 ± 0.69	9.09 ± 1.19	-
4	1.71 ± 0.45	0.67 ± 0.02	2.20 ± 0.29	1.80 ± 0.21
5	1.65 ± 0.26	1.05 ± 0.02	1.80 ± 0.32	0.38 ± 0.005
6	1.00 ± 0.22	1.69 ± 0.12	0.85 ± 0.02	2.91 ± 0.22
7	1.22 ± 0.12	0.57 ± 0.004	0.28 ± 0.004	-
8	1.09 ± 0.07	0.16 ± 0.05	0.48 ± 0.05	-
9	1.25 ± 0.22	1.06 ± 0.81	1.67 ± 0.59	-
10	8.32 ± 1.49	7.34 ± 2.73	3.91 ± 0.55	-

10 = [$AuPPh_3$(indole)]. IC_{50} (**L1**, **L2**, **L3**) >100μM in A549 cells, IC_{50} (dppe, dppp) >50 μM in Jurkat-pLTVHM cells, IC_{50} (**1**, **4**, **5** and [Au(indole)PPh_3]) = 11.7 ± 3.12, 2.81 ± 0.54, 2.58 ± 0.63 8.95 ± 2.08 respectively in HeLa cells.

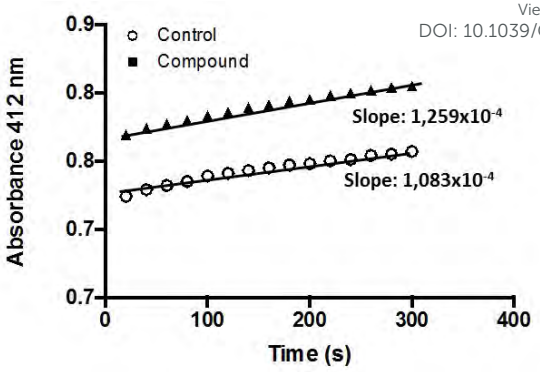

Fig 7. Inhibition of thioredoxin assay for complex **6**. Representation of the evolution of absorbance intensity of TNB during 5 minutes.

Experimental Section

Mass spectra were recorded on a BRUKER ESQUIRE 3000 PLUS, with the electrospray (ESI) technique. ^1H, $^{13}C\{H\}$ and ^{31}P NMR, including 2D experiments, were recorded at room temperature on a BRUKER AVANCE 400 spectrometer (^1H, 400 MHz, ^{13}C, 100.6 MHz, ^{31}P, 162 MHz) with chemical shifts (δ, ppm) reported relative to the solvent peaks of the deuterated solvent. Infrared spectra were recorded in the range 4000–250 cm^{-1} on a Perkin-Elmer Spectrum 100 FTIR spectrometer. Room temperature steady-state emission and excitation spectra were recorded with a Jobin-Yvon-Horiba fluorolog FL3-11 spectrometer fitted with a JY TBX picosecond detection module. UV/vis spectra were recorded with a 1 cm quartz cells on an Evolution 600 spectrophotometer.

Theoretical calculations.

For all calculations, with Gaussian 09,[36] we have used the PBEPBE density functional[37] and the solvent effects were introduced through the IEFPCM polarisable continuum model.[38] The pseudopotentials from Stuttgart,[39] and the corresponding basis sets augmented with two f polarization functions[40] were employed for the metal Au and def2-SVP basis set for all atoms.[41] Vibrational frequencies were calculated at the same theoretical level to confirm that each configuration was a minimum on the potential energy surface. The Supporting Information contains Cartesian coordinates for all optimised structures.

Crystal structure determinations

Crystals were mounted in inert oil on glass fibres and transferred to the cold gas stream of an Xcalibur Oxford Diffraction diffractometer equipped with a low-temperature attachment. Data were collected using monochromated MoKα radiation (λ = 0.71073 Å). Scan type ω. Absorption corrections based on multiple scans were applied using spherical harmonics implemented in SCALE3 ABSPACK scaling algorithm.[42] The structures were solved with the ShelXS structure solution program using direct methods and by using Olex2 as the graphical interface.[43] The model was refined using the program SHELXL.[44] All non-hydrogen atoms were

refined anisotropically. Further details on the crystal refinements are collected in Table S1. CCDC reference numbers 1818688 (**6**), 1818689 (**7**) and 1818690 (**8**).

Cytotoxicity assay

The MTT assay was used to determine cell viability as an indicator for cells sensitivity to the complexes. Exponentially growing cells A549, HeLa, Jurkat-pLVTHM, Jurkat-shBak and MEF fibroblast were seeded at a density of approximately 10^4 cells (A549) or $3x10^4$ cells (Jurkat-pLVTHM and Jurkat-shBak) per well in 96-well flat-bottomed microplates and allowed to attach (A549) or grow for 24 h prior to addition of compounds. The complexes were dissolved in DMSO and added to cells in concentrations ranging from 0.1 to 100 μM in quadruplicate. Cells were incubated with the compounds for 24 h at 37 °C. Ten microliters of MTT (5 mg ml^{-1}) were added to each well and plates were incubated for 2 h at 37 °C. Then, media was eliminated and DMSO (100 μl per well) was added to dissolve the formazan precipitates in the plates containing A549 and HeLa cells. Alternatively, plates containing either Jurkat-pLVTHM or Jurkat-shBak were previously centrifuged for 15 min at 2500 rpm. Thereafter, media was also eliminated and DMSO (100 μl per well) was added. The optical density was measured at 550 nm using a 96-well multiscanner autoreader (ELISA). The IC_{50} was calculated by nonlinear regression analysis using OriginPro8.

Thioredoxin inhibition assay. For determination of the thioredoxin reductase activity, A549 cells were incubated for 9 h with our compound at different concentrations near IC_{50} values. Cells were collected and washed with PBS and 150 μl buffer (1% Triton X-100, 150 mM NaCl, 50 mM Tris/HCl pH 7.6, 10% v/v glycerol, 1 mM EDTA, 1 mM sodium orthovanadate, 10 mM sodium pyrophosphate, 10 μg ml^{-1} leupeptin, 10 mM NaF, 1 mM sodium methylsulphonium) for 30 min at 0 °C, and centrifuged at 200 g for 10 min at 4 °C. The protein was quantified using the BCAprotein assay (Thermo Scientific) and 80 μg was added in each assay. Kinetic studies were performed in a buffer containing 0.2 M NaCl, H-phosphate pH 7.4, 2 mM EDTA, 0.25 mM NADPH and 3 mM DTNB. The increase in the absorbance was measured at 412 nm for 5 min at 25 °C.

Intracellular peroxides (ROS) formation. The production of ROS (Reactive Oxygen Species) was assessed using the dichlorofluorescein (DCF) assay.[45] Caco-2/TC7 cells were plated in 96-well plates at a density of 4000 cells perwell and incubated for 24 h under standard cell culture conditions. For treatment, **6** was added to cells within its IC_{50} concentration that of IC_{50} and incubated 24 h; mocktreated cells were just incubated with DMSO at the same concentration than treated cells. Then, cells were washed twice with PBS and 100 μL of 20 mM DCFH-DA (dichloro-dihydro-fluoresceindiacetate) were added to each well. Cells were incubated 1 h at 37 °C and washed twice with PBS; finally, 100 μL of PBS were added and fluorescence was analyzed with DTX-880 (Beckman Counter). Excitation and emission settings were 485 and 535 nm, respectively. The intensity of fluorescence is considered as a reflection of total intracellular ROS.

Materials and Procedures

The starting materials [AuCl(tht)], [Au_2Cl_2(μ-dppe)] and [Au_2Cl_2(μ-dppp)] were prepared according to literature procedures.[46] All other starting materials and solvents were purchased from commercial suppliers and used as received unless otherwise stated.

Compound 1. [AuCl(PPh_3)] (0.104 g, 0.211 mmol) was added to a solution of **L1** (0.030 g, 0.211 mmol) in 30 ml of DCM. Then, an excess of Cs_2CO_3 was added and the mixture was stirred at r.t. for 24 h. Thereafter, the mixture was filtered through celite and the solvent was removed at high vacuum affording a white solid (0.063 g, 50%). ^{1}H NMR (400 MHz, $CDCl_3$) δ 7.87 (d, *J* = 8.1 Hz, 1H, C*H*(7)), 7.64-7.49 (m, 16H, C*H*(Ph), C*H*(2)), 7.36–7.33 (m, 1H, C*H*(5)), 7.05 (dd, *J* = 8.0, 7.4 Hz, 1H, C*H*(6)), 6.76-6.74 (m, 1H, C*H*(3)). ^{31}P (162 MHz, $CDCl_3$): δP 31.3; ^{13}C NMR (101 MHz, $CDCl_3$) δC 144.6 (s, 1C, *C*(7a)), 138.8 (s, 1C, *C*(2)), 134.3 (d, *J* = 13.7 Hz, 6C, *C*($_{orto}$-Ph)), 132.1 (d, *J* = 2.5 Hz, 3C, *C*($_{para}$-Ph), 130.8 (s, 1C, C(3a)), 129.5 (d, *J* = 11.6 Hz, 6C, C($_{meta}$-Ph), 129.1 (d, *J* = 59.9 Hz, 3C, *C*($_{ipso}$-Ph)), 123.8 (s, 1C, *C*(5)), 120.5 (s, 1C, *C*N), 119.3 (s, 1C, *C*(7)), 118.6 (s, 1C, *C*(6)), 101.6 (s, 1C, *C*(4)), 100.0 (s, 1C, *C*(3)). MS (ESI$^+$): m/z, 601.2 ([MH]$^+$, 4.3%), calculated 601.1. IR, υ(solid, cm^{-1}): 2213 (CN).

Compound 2. Compound **2** was synthesized following an analogous procedure to that of complex **1.** Its experimental data agrees with that already reported somewhere else.[19]

Compound 3. This compound was prepared similarly to **1** using **L3** instead of **L1**. The product was obtained as a maroon solid (0.072 g, 66% yield). ^{1}H NMR (400 MHz, $CDCl_3$) δ 7.53 (m, 15H, C*H*(Ph)), 7.13 (s, 1H, C*H*(4)), 7.00 (s, 1H, C*H*(6)), 2.51 (s, 3H, CH_3(B)), 2.20 (s, 3H, CH_3(A)). ^{31}P (162 MHz, $CDCl_3$): δP 32.1; ^{13}C NMR (101 MHz, $CDCl_3$) δC 189.7 (s, 1C, *CO*(3), 167.8 (s, 1C, *CO*(2)), 157.6 (s, 1C, *C*(7a)), 140.6 (s, 1C, *C*(6)), 134.2 (d, *J* = 13.6 Hz, 6C, *C*($_{orto}$-Ph)), 132.0 (d, *J* = 2.1 Hz, 3C, *C*($_{para}$Ph)), 130.2 (s, 1C, *C*(3a)), 129.3 (d, *J* = 11.7 Hz, 6C, *C*($_{meta}$-Ph), 128.9 (d, *J* = 61.6 Hz, 3C, *C*($_{ipso}$Ph)), 122.7 (s, 1C, *C*(4)), 122.1 (s, 1C, *C*(5)), 120.9 (s, 1C, *C*(7)), 20.4 (s, 2C, *C*H$_3$(A)), 19.2 (s, 2C, *C*H$_3$(B)). MS (ESI$^+$): m/z, 634.1 ([MH]$^+$, 24.8%), calculated 634.1. IR, υ(solid, cm^{-1}): 1719, 1679, 1615 (CO).

Compound 4. [Au_2Cl_2(μ-dppe)] (0.100 g, 0.115 mmol) was added to a solution of **L1** (0.033 g, 0.232 mmol) in 30 ml of DCM. Then, an excess of Cs_2CO_3 was added and the mixture was stirred at r.t. for 24 h. Thereafter, the mixture was filtered through celite and the solvent was removed at high vacuum affording a white solid (0.052 g, 49%). ^{1}H NMR (400 MHz, $CDCl_3$) δ 7.78-7.62 (m, 10H, C*H*(7), C*H*(Ph)), 7.60-7.56 (m, 4H, C*H*(Ph)), 7.53-7.47 (m, 8H, C*H*(Ph)), 7.43 (d, *J* = 2.3 Hz, 2H, C*H*(2)), 7.35 (dd, *J* = 7.3, 0.8 Hz, 2H, C*H*(5)), 7.04-6.93 (m, 2H, C*H*(6)), 6.75 (d, *J* = 2.3 Hz, 2H, C*H*(3)), 2.85 (d, *J* = 2.2 Hz, 4H, C*H*(9)); ^{31}P (162 MHz, $CDCl_3$): δP 30.4; ^{13}C NMR (101 MHz, $CDCl_3$) δC 138.7 (s, 2C, *C*(2)), 133.3 (t, *J* = 6.7 Hz, 8C, *C*($_{orto}$-Ph)), 133.0 (s, 4C, *C*($_{para}$-Ph)), 130.0 (t, *J* = 5.8 Hz, 8C, *C*($_{meta}$-Ph)), 123.9 (s, 2C, *C*(5)), 120.4 (s, 2C, *C*(7a)), 119.0 (s, 2C, *C*(7)), 118. (s, 2C, *C*(6)), 101.8 (s, 2C, *C*(4)), 100.4 (s, 2C, *C*(3)). MS (ESI$^+$):

m/z, 1074.2 ([MH]$^+$, 0.7%), calculated 1074.2, 933.3 ([M – L1]$^+$, 8%), calculated 933.1. IR, υ(solid, cm^{-1}): 2208 (CN).

Compound 5. [Au_2Cl_2(μ-dppp)] (0.093 g, 0.105 mmol) was added to a solution of **L1** (0.030 g, 0.211 mmol) in 30 ml of DCM. Then, an excess of Cs_2CO_3 was added and the mixture was stirred at r.t. for 24 h. Thereafter, the mixture was filtered through celite and the solvent was removed at high vacuum affording a white solid (0.058 g, 50 %). ^{1}H NMR (400 MHz, $CDCl_3$) δ 7.70 (d, *J* = 8.1 Hz, 2H, C*H*(7)), 7.62-7.53 (m, 8H, CH_{meta}(Ph)), 7.51-7.44 (m, 4H, CH_{para}(Ph)), 7.40-7.29 (m, 6H, CH_{orto}(Ph), C*H*(5, 2)), 6.99-6.82 (m, 2H, C*H*(6)), 6.68 (d, *J* = 2.5 Hz, 2H, C*H*(3)), 2.91 (dt, *J* = 10.3, 7.0 Hz, 4H, C*H*(9)), 2.12-1.93 (m, 2H, C*H*(10)). ^{31}P (162 MHz, $CDCl_3$): δP 23.4; ^{13}C NMR (101 MHz, $CDCl_3$) δC 144.5 (s, 2C, *C*(7a)), 139.0 (s, 2C, *C*(2)), 133.2 (d, *J* = 13.0 Hz, 8C, *C*($_{orto}$-Ph)), 132.5 (d, *J* = 2.3 Hz, 4C, *C*($_{para}$-Ph)), 131.0 (s, 2C, *C*(3a)), 129.7 (d, *J* = 11.5 Hz, 8C, *C*($_{meta}$-Ph)), 128.2 (d, *J* = 60.0 Hz, 4C, *C*($_{ipso}$-Ph)), 123.8 (s, 2C, *C*(5)), 121.1 (d, *J* = 121.2 Hz, 2C, *C*N), 119.2 (s, 2C, *C*(7)), 118.7 (s, 2C, *C*(6)), 101.5 (s, 2C, *C*(4)), 100.2 (s, 2C, *C*(3)), 27.9 (dd, *J* = 37.9, 10.6 Hz, 2C, *C*(A)), 19.9 (s, 1C, *C*(B)). MS (ESI$^+$): m/z, 947.0 ([M – L1]$^+$, 100%), calculated 947.1. IR, υ(solid, cm^{-1}): 2208 (CN).

Compound 6. This compound was prepared similarly to **4** using **L2** instead of **L1**. The product was obtained as an orange solid (0.104 g, 83% yield). ^{1}H NMR (400 MHz, $CDCl_3$) δ 7.80-7.73 (m, 8H, CH_{ortho}(Ph)), 7.57-7.41 (m, 12H, C$H_{para,\ meta}$(Ph)), 7.20 (td, *J* = 7.7, 1.4 Hz, 2H, C*H*(6)), 7.05 (d, *J* = 7.3 Hz, 2H, C*H*(4)), 6.76 (d, *J* = 7.7 Hz, 2H, C*H*(7)), 6.68 (td, *J* = 7.5, 0.8 Hz, 2H, C*H*(5)), 2.92-2.73 (m, 4H, CH_2(A)). ^{31}P (162 MHz, $CDCl_3$): δP 26.6. ^{13}C NMR (101 MHz, $CDCl_3$) δC 189.3 (s, 2C, *CO*(3)), 166.7 (s, 2C, *CO*(2)), 160.7 (s, 2C, *C*(7a)), 138.4 (s, 2C, *C*(6)), 133.5 (t, *J* = 6.7 Hz, 8C, *C*($_{orto}$-Ph)), 132.5 (s, 4C, *C*($_{para}$-Ph)), 129.9 (t, *J* = 5.8 Hz, 8C, *C*($_{meta}$-Ph)), 127.8 (dd, *J* = 66.8, 6.9 Hz, 4C, *C*($_{ipso}$-Ph)), 124.2 (s, 2C, *C*(4)), 121.5 (s, 2C, *C*(5)), 119.8 (s, 2C, *C*(3a)), 113.9 (s, 2C, *C*(7)), 23.9 (d, *J* = 38.51 Hz, 2C, *C*H_2(A)). MS (ESI$^+$): m/z, 638.1 ([M – L2]$^+$, 100%), calculated 638.1. IR, υ(solid, cm^{-1}): 1726, 1682, 1601 (CO).

Compound 7. This compound was prepared similarly to **5** using **L2** instead of **L1**. The product was obtained as a maroon solid (0.066 g, 59% yield). ^{1}H NMR (400 MHz, $CDCl_3$) δ 7.80-7.63 (m, 8H, CH_{ortho}(Ph)), 7.53-7.44 (m, 12H, C$H_{meta\ /\ para}$(Ph)), 7.28-7.18 (m, 4H, C*H*(6, 4)), 6.80- 6.70 (m, 4H, C*H*(7, 5)), 2.92 (dt, *J* = 10.4, 7.0 Hz, 4H, CH_2(A)), 2.01 (ddd, *J* = 23.8, 16.6, 7.0 Hz, 2H, CH_2(B)). ^{31}P (162 MHz, $CDCl_3$): δP 25.4. ^{13}C NMR (101 MHz, $CDCl_3$) 189.5 (s, 2C, *CO*(3)) 166.7 (s, 2C, *CO*(2)), 161.7 (s, 2C, *C*(7a)), 138.1 (s, 2C, *C*(6)), 133.5 (d, *J* = 13.0 Hz, 8C, *C*($_{orto}$-Ph)), 132.4 (d, *J* = 2.4 Hz, 4C, *C*($_{para}$-Ph)), 129.7 (d, *J* = 11.6 Hz, 8C, *C*($_{meta}$-Ph)), 128.4 (d, *J* = 60.3 Hz, 4C, *C*($_{ipso}$-Ph)), 124.6 (s, 2C, *C*(4)), 121.5 (s, 2C, *C*(5)), 120.3 (s, 2C, *C*(3a)), 114.1 (s, 2C, *C*(7)), 28.0 (dd, *J* = 37.6, 10.0 Hz, 2C, *C*H_2(A)), 20.1 (s, 1C, *C*H_2(B)). MS (ESI$^+$): m/z, 952.1 ([M – L2]$^+$, 100%), calculated 952.1. IR, υ(solid, cm^{-1}): 1726, 1682, 1602 (CO).

Compound 8 This compound was prepared similarly to **4** using **L3** instead of **L1**. The product was obtained as a red solid (0.108 g, 82% yield). ^{1}H NMR (400 MHz, $CDCl_3$) δ 7.84-7.72 (m, 8H, CH_{ortho}(Ph)), 7.55-7.47 (m, 12H, C$H_{meta/para}$(Ph)), 6.84 (s, 2H, C*H*(6)), 6.76 (s, 2H, C*H*(4)), 2.83 (d, *J* = 7.2 Hz, 4H, CH_2(C)), 2.61 (s, 6H, CH_3(B)), 2.41 (s, 6H, CH_3(A)). ^{31}P (162 MHz, $CDCl_3$): δP 27.4. ^{13}C NMR (101 MHz, $CDCl_3$) 189.8 (s, 2C, *CO*(3)), 167.4 (s, 2C, *CO*(2)), 156.9 (s, 2C, *C*(7a)), 141.0 (s, 2C, *C*(6)), 133.5 (t, *J* = 6.7 Hz, 8C, *C*($_{orto}$-Ph)), 132.4 (s, 4C, *C*($_{para}$-Ph)), 130.4 (s, 2C, *C*(3a)), 129.8 (t, *J* = 5.8 Hz,8C, *C*($_{meta}$-Ph)), 128.4 (d, *J* = 59.9 Hz, 4C, *C*($_{ipso}$-Ph)), 122.3 (s, 2C, *C*(4)), 121.9 (s, 2C, *C*(5)), 120.6 (s, 2C, *C*(7)), 24.3 (d, *J* = 40.0 Hz, 2C, *C*H_2(C)), 20.5 (s, 2C, *C*H_3(A)), 19.1 (s, 2C, *C*H_3(B)). MS (ESI$^+$): m/z, 966.1 ([M – L3]$^+$, 100%), calculated 966.1. IR, υ(solid, cm^{-1}): 1730, 1669, 1616 (CO).

Compound 9. This compound was prepared similarly to **5** using **L2** instead of **L1**. The product was obtained as a dark red solid (0.064 g, 65% yield). ^{1}H NMR (400 MHz, $CDCl_3$) δ 7.76-7.68 (m, 8H, CH_{ortho}(Ph)), 7.52-7.41 (m, 12H, C$H_{meta/para}$(Ph)), 6.94 (s, 2H, C*H*(6)), 6.81 (s, 2H, C*H*(4)), 2.98-2.89 (m, 4H, CH_2(C)), 2.29 (s, 6H, CH_3(B)), 2.16 (s, 6H, CH_3(A)), 2.09-1.92 (m, 2H, CH_2(D)). ^{31}P (162 MHz, $CDCl_3$): δP 25.0. ^{13}C NMR (101 MHz, $CDCl_3$) 189.7 (s, 2C, *CO*(3)), 167.5 (s, 2C, *CO*(2)), 157.2 (s, 2C, *C*(7a)), 140.7 (s, 2C, *C*(6)), 133.4 (d, *J* = 13.0 Hz, 8C, *C*($_{orto}$-Ph)), 132.1 (s, 4C, *C*($_{para}$-Ph)), 129.5 (d, *J* = 11.5 Hz, 8C, *C*($_{meta}$-Ph)), 128.8 (d, *J* = 60.17 Hz, 4C, *C*($_{ipso}$-Ph)), 122.4 (s, 2C, *C*(4)), 122.0 (s, 2C, *C*(5)), 120.6 (s, 2C, *C*(7)), 27.8 (d, *J* = 44.1 Hz, 2C, CH$_2$(C)), 20.4 (s, 2C, *C*H_3(A)), 20.3 (s, 1C, *C*H_2(D)), 19.0 (s, 2C, *C*H_3(B)). MS (ESI$^+$): m/z, 980.1 ([M – L3]$^+$, 100%), calculated 980.1. IR, υ(solid, cm^{-1}): 1722, 1678, 1615 (CO).

Conclusions

In summary, we have reported the synthesis of luminescent monometallic [AuLPPh$_3$] (**1**-**3**) and bimetallic [Au_2(μ-dppe)L_2] (**4**, **6**, **8**) and [Au_2(μ-dppp)L_2] (**5**, **7**, **9**) complexes, where L is either 4-cyanoindole, isatin, or 5,7-dimethyl-isatin. Structural characterisation by X-ray diffraction showed the expected linear disposition around the gold metal centre as well as the predisposition to form intramolecular aurophilic interactions for those complexes containing dppe as bridge ligand. All complexes displayed a similar emission profile around 400 nm. Theoretical calculations revealed that the origin of the emission was dependent on the nature of the heterocycle. Thus, in the case of the indole derivatives a mixture of LLCT and LMCT seemed to be the source of the emission, whereas an IL (isatin based) and a LMCT transitions in the case of the isatin derivatives. Additionally, the lifetimes in the range of hundreds of nanoseconds suggests the fluorescence nature of the emissions. As result of these data, i.e. the high-energy excitation and emission as well as the short lifetimes, these complexes cannot be considered suitable for cell imaging purposes. In contrast, cell antiproliferative assays performed in lung cancer (A549), cervix cancer (HeLa), leukemia Jurkat-pLVTHM and Jurkat-shBak cells showed a similar cytotoxic behaviour for the three families of complexes, being the bimetallic species at least twice as toxic as the monometallic, with IC_{50} values between 10.11 and 0.28 μM. Additional MTT assays performed to the free ligands **L1**-**L3** and dppe and dppp ligands point towards the metal centre as the main responsible of such cytotoxicity. Initial studies on thioredoxin inhibition and reactive oxygen species suggest a different biological target than that of thioredoxin for these gold complexes. Although these are preliminary studies, the fact that the

synthesised complexes inhibit the cell proliferation of both, leukemia Jurkat-pLVTHM and Jurkat-shBak cells, cisplatin sensitive and resistant cells respectively, suggest the novel complexes as an alternative cisplatin drug for the treatment of this specific disease.

Conflicts of interest

There are no conflicts to declare.

Acknowledgements

Authors thank the Ministerio de Economía y Competitividad (MINECO-FEDER CTQ2016-75816-C2-1-P, CTQ2017-88091-P and Gobierno de Aragón-Fondo Social Europeo (E77) for financial support. Moreover, they thank Galicia Supercomputing Technological Center (CESGA-CSIC), Spain, for the computer resources provided.

Notes and references

1 a) L. Fu, *Top. Heterocycl. Chem.,* 2010, **26**, 433; b) A. J. Kochanowska-Karamyan and M. T. Hamann, *Chem. Rev.*, 2010, **110**, 4489; c) S. Lancianesi, A. Palmieri, M. Petrini, *Chem. Rev.*, 2014, **114**, 7108.

2 a) Y.-J. Wu, *Top. Heterocycl. Chem.,* 2010, **26**, 1; b) S. M. Bronner, G. Y. J. Im and N. K. Garg, *Heterocycles in Natural Product Synthesis*. Wiley-VCH, Verlag GmbH & Co. KGaA, 2011, pp. 221; c) N. K. Kaushik, N. Kaushik, P. Attri, N. Kumar, C. H. Kim, A. K. Verma and E. H. Choi, *Molecules,* 2013, **18**, 6620; d) M.-Z. Zhang, Q. Chen and G.-F. Yang, *Eur. J. Med. Chem.,* 2015, **89**, 421.

3 M. Bandini and A. Eichholzer, *Angew. Chem. Int. Ed.*, 2009, **48**, 9608.

4 For selected reviews, see: a) E. Marqués-López, A. Diez-Martinez, P. Merino and R. P. Herrera, *Curr. Org. Chem.,* 2009, **13**, 1585; b) D. F. Taber and P. K. Tirunahari, *Tetrahedron,* 2011, **67**, 7195; c) M. Shiri, *Chem. Rev.,* 2012, **112**, 3508; d) N. Yoshikai and Y. Wei, *Asian J. Org. Chem.,* 2013, **2,** 466; e) M. Inman and C. J. Moody, *Chem. Sci.,* 2013, **4**, 29; f) G. Bartoli, R. Dalpozzo and M. Nardi, *Chem. Soc. Rev.*, 2014, **43**, 4728; g) R. Dalpozzo, *Chem. Soc. Rev.*, 2015, **44**, 742.

5 For selected reviews, see: a) B. M. Trost and M. K. Brennan, *Synthesis,* 2009, 3003; b) F. Zhou, Y.-L. Liu and J. Zhou, *Adv. Synth. Catal.,* 2010, **352**, 1381; c) N. Lashgari and G. M. Ziarani, *Arkivoc,* 2012**,** (**i**), 277; d) N. R. Ball-Jones, J. J. Badillo and A. K. Franz, *Org. Biomol. Chem*., 2012, **10**, 5165; e) S. Mohammadi, R. Heiran, R. P. Herrera and E. Marqués-López, *ChemCatChem*, 2013, **5**, 2131; f) G. Mathur and S. Nain, *Med. Chem.,* 2014, **4**, 417.

6 a) T. Ohshima, *Chem. Pharm. Bull.,* 2004, **52**, 1031; b) V. Sharma, P. Kumar and D. Pathak, *J. Heterocyclic Chem.*, 2010, **47**, 491; c) S. Biswal, U. Sahoo, S. Sethy, H. K. S. Kumar and M. Banerjee, *Asian J. Pharm. Clin. Res.,* 2012*,* **5**, 1.

7 R. F. Vasil'ev, A. V. Trofimov and Y. B. Tsaplev, *Russ. Chem. Rev.,* 2010, **79**, 77.

8 a) L. Ortego, M. Meireles, C. Kasper, A. Laguna, M. D. Villacampa and M. C. Gimeno, *J. Inorg. Biochem.*, 2016, **156**, 133; b) L. Ortego, A. Laguna, J. Gonzalo-Asensio, M. D. Villacampa and M. C. Gimeno, *J. Inorg. Biochem.,* 2015, **146**, 19; c) A. Gutiérrez, I. Marzo, C. Cativiela, A. Laguna and M. C. Gimeno, *Chem. Eur. J.*, 2015, **21**, 11088; d) H. Goitia, Y. Nieto, M. D. Villacampa. C. Casper, A. Laguna, M. C. Gimeno, *Organometallics*, 2013, **32**, 6069.

9 a) A. Luengo, V. Fernández-Moreira, I. Marzo and M. C. Gimeno, *Inorg Chem.,* 2017, **56**, 15159; b) R. Visbal, V. Fernández-Moreira, I. Marzo, A. Laguna and M. C. Gimeno, *Dalton Trans.,* 2016, **45**, 15026; c) V. Fernández-Moreira, I. Marzo and M. C. Gimeno, *Chem. Sci.*, 2014, **5**, 4434.

10 For the scarce examples reported, see: a) D. V. Partyka, M. Zeller, A. D. Hunter and T. G. Gray, *Inorg. Chem.,* 2012, **51**, 8394; b) K. J. Kilpin, W. Henderson and B. K. Nicholson, *Polyhedron,* 2007, **26**, 207; c) S. Craig, L. Gao, I. Lee, T. Gray and A. J. Berdis, *J. Med. Chem.,* 2012, **55**, 2437; d) M. C. Gimeno, H. Goitia, A. Laguna, M. E. Luque, M. D. Villacampa, C. Sepúlveda and M. Meireles, *J. Inorg. Biochem*., 2011, **105**, 1373.

11 P. Štarha, Z. Trávníček, B. Drahoš and Z. Dvořák, *Int. J. Mol. Sci.,* 2016, **17**, 2084.

12 Z. Trávníček, P. Štarha, J. Vančo, T. Šilha, J. Hošek, P. Suchý, Jr., and G. Pražanová, *J. Med. Chem.*, 2012, **55**, 4568.

13 J. Hošek, J. Vančo, P. Štarha, L. Paráková, Z. Trávníček, *PLOS ONE*, 2013, **8**, e82441.

14 J. Vančo, J. Gáliková, J. Hošek, Z. Dvořák, L. Paráková and Z. Trávníček, *PLOS ONE*, 2014, **9**, e109901.

15 a) D. Hu, Y. Liu, Y.-T. Lai, K.-C. Tong, Y.-M. Fung, C.-N. Lok, and C.-M. Che, *Angew. Chem. Int. Ed.,* 2016, **55**, 1387; b) C. Martín-Santos, E. Michelucci, T. Marzo, L. Messori, P. Szumlas, P. J. Bednarski, R. Mas-Ballesté, C. Navarro-Ranninger, S. Cabrera and J. Alemán, *J. Inorg. Biochem.,* 2015, **153**, 339; c) B. Đ. Glišić, U. Rychlewska and M. I. Djuran, *Dalton Trans.,* 2012, **41**, 6887; d) R. W.-Y. Sun and C.-M. Che, *Coord. Chem. Rev.,* 2009, **253**, 1682.

16 a) E. Garcia-Moreno, S. Gascon, J. A. Garcia de Jalón, E. Romanos, M. J. Rodríguez-Yoldi, E. Cerrada and M. Laguna, *Anticancer Agents Med. Chem.*, 2015, **15**, 773; b) L. Ortego, F. Cardoso, S. Martins, M. F. Fillat, A. Laguna, M. Meireles, M. D. Villacampa and M. C. Gimeno, J. *Inorg. Biochem*., 2014, **130**, 32; c) A. Gutiérrez, L. Gracia-Fleta, I. Marzo, C. Cativiela, A. Laguna and M. C. Gimeno, *Dalton Trans.,* 2014, **43**, 17054; d) E. R. T. Tiekink, *Bioinorg. Chem. Appl.*, 2003, **1**, 53.

17 For some use and transformations of **L1**, see: a) S. Enthaler, K. Junge, D. Addis, G. Erre and M. Beller, *ChemSusChem,* 2008, **1**, 1006; b) D. Robaa, C. Enzensperger, S. El Din Abul Azm, E. S. El Khawass, O. El Sayed and J. Lehmann, *J. Med. Chem.,* 2010, **53**, 2646; c) M. Zhang and W. Tang, *Org. Lett.,* 2012, ***14***, 3756; d) H. Kinuta, Y. Kita, E. Rémond, M. Tobisu and N. Chatani, *Synthesis,* 2012, 2999; e) C. Mateos, J. A. Rincón and J. Villanueva, *Tetrahedron Lett.,* 2013, **54**, 2226; f) M. Vilches-Herrera, S. Werkmeister, K. Junge, A. Börner and M. Beller, *Catal. Sci. Technol*., 2014, **4**, 629.

18 a) I. Chiyanzu, E. Hansell, J. Gut, P. J. Rosenthal, J. H. McKerrow and K. Chibale, *Bioorg. Med. Chem. Lett.,* 2003, **13**, 3527; b) J. L. Hyatt, T. Moak, M. J. Hatfield, L. Tsurkan, C. C. Edwards, M. Wierdl, M. K. Danks, R. M. Wadkins and P. M. Potter, *J. Med. Chem.,* 2007**, 50***,* 1876; c) R. Dutt, M. Singh and A. K. Madan, *Med. Chem. Res.,* 2012*,* **21**, 1226.

19 A. Lenz, K. Slinkel and W. Beck, *Z. Naturforsch*., 1996, **51b,** 1639.

20 U. E. I. Horvath, L. Dobrzańska, C. E. Strasser, W. Bouwer (neé Potgieter), G. Joone, C. E. J. van Rensburg, S. Cronje and H. G. Raubenheimer, *J. Inorg. Biochem.,* 2012, **111**, 80.

21 a) R. Narayanaswamy, M. A. Young, E. Parkhurst, M. Oullette, M. E. Kerr, D. M. Ho, R. C. Elder, A. E. Bruce and M. R. M. Bruce, *Inorg. Chem.,* 1993, **32**, 2506; b) E. Colacio, R. Cuesta, J. M. Gutiérrez-Zorrilla, A. Luque, P. Román, T. Giraldi and M. R. Taylor, *Inorg. Chem.*, 1996, **35**, 4232.

22 H. Friebolin, Basic *One- and Two-Dimensional NMR Spectroscopy*, Wiley-VCH, Weinheim, 1998, pp. 124-125.

23 M. F. M. Monzittu, V. Fernández-Moreira, V. Lippolis, M. Arca, A. Laguna and M. C. Gimeno, *Dalton Trans.,* 2014, **43**, 6212.
24 a) H. Schmidbaur, *Chem. Soc. Rev.,* 1995, **24**, 391; b) L. Hao, R. J. Lachicotte, H. J. Gysling and R. Eisenberg, *Inorg. Chem*., 1999, **38**, 4616; c) H. Schmidbaur and A. Schier, *Chem Soc. Rev*., 2012, **41**, 370.
25 a) C. Janiak, *J. Chem. Soc., Dalton Trans.*, 2000, 3885; b) O. Crespo, M. C. Gimeno, A. Laguna, S. Montanel-Pérez, and M. D. Villacampa, *Organometallics*, 2012, **31**, 5520.
26 P. Berci-Filho, F. H. Quina, M. H. Gehlen, M. J. Politi, M. G. Neumann and T. C. Barros, *J. Photochem. Photobiol. A,* 1995, **92**, 155.
27 T. Polat, F. Bulut, I. Arıcan, F. Kandemirli and G. Yildirim, *J. Mol. Struct.,* 2015, **1101**, 189.
28 K. T. Chan, G. S. M. Tong, W.-P. To, C. Yang, L. Du, D. L. Phillips and C.-M. Che, *Chem. Sci.*, 2017, **8**, 2352.
29 a) F. C. Uhle, *J. Am. Chem. Soc.,* 1949, **71**, 761; b) G. S. Ponticello and J. J. Baldwin, *J. Org. Chem.*, 1979, **44**, 4003; c) H. Maehr and J. M. Smallheer *J. Org. Chem.*, 1981, **46**, 1752.
30 I. Fleming (Ed.) Frontier Orbitals and Organic Chemical Reactions, Wiley, London, 1976.
31 L. Vela, M. Contel, L. Palomera, G. Azaceta and I. Marzo, *J. Inorg. Biochem.*, 2011, **105**, 1306.
32 S. Das, S. Sinha, R. Britto, K. Somasundaram and A. G. Samuelson, *J. Inorg. Biochem.,* 2010, **104**, 93.
33 a) S. Gromer, L. D. Arscott, C. H. Williams, Jr., R. H. Schirmer and K Becker, *J. Biol. Chem.,* 1998, **273**, 20096; b) S. Urig, K. Fritz-Wolf, R. Réau, C. Herold-Mende, K. Tóth, E. Davioud-Charvet and K. Becker, *Angew. Chem. Int. Ed.,* 2006, **45**, 1881; c) I. Ott, *Coord. Chem. Rev.,* 2009, **253**, 1670; d) S. Nobili, E. Mini, I. Landini, C. Gabbiani, A. Casini and L. Messori, *Med. Res. Rev.*, 2010, **30**, 550.
34 M. Frik, J. Fernández-Gallardo, O. Gonzalo, V. Mangas-Sanjuan, M. González-Alvarez, A. Serrano del Valle, C. Hu, I. González-Alvarez, M. Bermejo, I. Marzo, and M. Contel, *J. Med. Chem.*, 2015, **58**, 5825.
35 B. Cunniff, G. W.; Snider, N. Fredette, R. J. Hondal and N. H Heintz *Anal. Biochem.* 2013, **443**, 34.
36 M. J. Frisch, G. W. Trucks, H. B. Schlegel, G. E. Scuseria, M. A. Robb, J. R. Cheeseman, G. Scalmani, V. Barone, B. Mennucci, G. A. Petersson, H. Nakatsuji, M. Caricato, X. Li, H. P. Hratchian, A. F. Izmaylov, J. Bloino, G. Zheng, J. L. Sonnenberg, M. Hada, M. Ehara, K. Toyota, R. Fukuda, J. Hasegawa, M. Ishida, T. Nakajima, Y. Honda, O. Kitao, H. Nakai, T. Vreven, J. A. Jr. Montgomery, J. E. Peralta, F. Ogliaro, M. Bearpark, J. J. Heyd, E. Brothers, K. N. Kudin, V. N. Staroverov, R. Kobayashi, J. Normand, K. Raghavachari, A. Rendell, J. C. Burant, S. S. Iyengar, J. Tomasi, M. Cossi, N. Rega, J. M. Millam, M. Klene, J. E. Knox, J. B. Cross, V. Bakken, C. Adamo, J. Jaramillo, R. Gomperts, R. E. Stratmann, O. Yazyev, A. J. Austin, R. Cammi, C. Pomelli, J. W. Ochterski, R. L. Martin, K. Morokuma, V. G. Zakrzewski, G. A. Voth, P. Salvador, J. J. Dannenberg, S. Dapprich, A. D. Daniels, Ö. Farkas, J. B. Foresman, J. V. Ortiz, J. Cioslowski and D. J. Fox, Gaussian 09, Revision A.1; Gaussian Inc., Wallingford CT, 2009.
37 C. Adamo and V. Barone, *J. Chem. Phys.*, 1999, **110**, 6158.
38 G. Scalmani and M. J. Frisch, *J. Chem. Phys.*, 2010, **132,** 114110.
39 D. Andrae, U. Häußermann, M. Dolg, H. Stoll and H. Preuß, *Theor. Chim. Acta*, 1990, ***77***, 123.
40 P. Pyykkö, N. Runeberg and F. Mendizabal*, Chem. Eur. J.*, 1997, **3**, 1451.
41 a) A. Schäfer, H. Horn and R. Ahlrichs, *J. Chem. Phys.,* 1992, **97**, 2571; b) F. Weigend and R. Ahlrichs, *Phys. Chem. Chem. Phys.,* 2005, **7**, 3297.
42 CysAlisPro, Version 1.171.35.11; Agilent Technologies. Multiscan absorption correction with SCALE3 ABSPACK scaling algorithm.
43 O. V. Dolomanov, L. J. Bourhis, R. J. Gildea, J. A. K. Howard, and H. Puschmann, *J. Appl. Cryst.*, 2009, **42**, 339-341.
44 G. M. Sheldrick, *Acta Cryst. Sect. C,* 2015, **71**, 3.
45 M. Ruiz-Leal, S. George, *Mar. Environ. Res.*, 2004, **58**, 631–635.
46 a) R. Uson and A. Laguna, *Organomet. Synth.,* 1985, **3**, 325; b) L. Malatesta, L. Naldini, G. Simonetta and F. Cariati, *Coord. Chem. Rev.,* 1966, **1**, 255.

View Article Online
DOI: 10.1039/C8DT00298C

Graphical Abstract

Bioactive and luminescent indole and isatin based gold(I) derivatives

Vanesa Fernández-Moreira,* Cynthia Val-Campillo, Isaura Ospino, Raquel P. Herrera, Isabel Marzo, Antonio Laguna and M. Concepción Gimeno*

Combination of bioactive indole and isatin derivatives with Au(I) affords highly cytotoxic metallic species even for cisplatin resistant leukemia cells (Jurkat-shBak).